Efficient and accurate determination of lattice-vacancy diffusion coefficients via non equilibrium ab initio molecular dynamics

Davide Sangiovanni, Olle Hellman, Björn Alling and Igor Abrikosov

Original Publication:

Davide Sangiovanni, Olle Hellman, Björn Alling and Igor Abrikosov, Efficient and accurate determination of lattice-vacancy diffusion coefficients via non equilibrium ab initio molecular dynamics, 2016, PHYSICAL REVIEW B, (93), 9, 094305.
http://dx.doi.org/10.1103/PhysRevB.93.094305

Efficient and accurate determination of lattice-vacancy diffusion coefficients via non equilibrium *ab initio* molecular dynamics

D. G. Sangiovanni,[1,*] O. Hellman,[1] B. Alling,[1,2] and I. A. Abrikosov[1,3,4]
[1]*Department of Physics, Chemistry and Biology (IFM), Linköping University, SE-58183 Linköping, Sweden*
[2]*Max-Planck-Institut für Eisenforschung GmbH, D-402 37 Düsseldorf, Germany*
[3]*Materials Modeling and Development Laboratory, National University of Science and Technology 'MISIS', 119049 Moscow, Russia*
[4]*LACOMAS Laboratory, Tomsk State University, 634050 Tomsk, Russia*
(Received 21 September 2015; revised manuscript received 27 January 2016; published 21 March 2016)

We revisit the color-diffusion algorithm [Aeberhard *et al.*, Phys. Rev. Lett. **108**, 095901 (2012)] in non equilibrium *ab initio* molecular dynamics (NE-AIMD) and propose a simple efficient approach for the estimation of monovacancy jump rates in crystalline solids at temperatures well below melting. Color-diffusion applied to monovacancy migration entails that one lattice atom (colored atom) is accelerated toward the neighboring defect site by an external constant force **F**. Considering bcc molybdenum between 1000 and 2800 K as a model system, NE-AIMD results show that the colored-atom jump rate k_{NE} increases exponentially with the force intensity F, up to F values far beyond the linear-fitting regime employed previously. Using a simple model, we derive an analytical expression which reproduces the observed $k_{\mathrm{NE}}(F)$ dependence on F. Equilibrium rates extrapolated by NE-AIMD results are in excellent agreement with those of unconstrained dynamics. The gain in computational efficiency achieved with our approach increases rapidly with decreasing temperatures and reaches a factor of 4 orders of magnitude at the lowest temperature considered in the present study.

DOI: 10.1103/PhysRevB.93.094305

I. INTRODUCTION

Point defects, such as lattice vacancies, affect the chemical, structural, mechanical, optical, and electronic properties of crystalline solids [1,2]. Transition-state theory (TST) [3], routinely used to extrapolate finite-temperature vacancy jump rates from migration energies and attempt frequencies calculated at 0 K [4], provides reliable point-defect diffusivities for temperatures at which the lattice vibrations remain essentially harmonic [5]. However, the modifications induced by the collective atomic motion on the effective potential-energy landscape, which in turn controls atomic mobilities, become progressively more significant for increasing temperatures [6–8]. Moreover, diffusion parameters calculated at 0 K are not reliable for crystal structures which are stable at finite temperatures due to anharmonic lattice vibrations, whereas exhibit imaginary phonon frequencies at 0 K [9,10]. This results in molecular dynamics (MD) becoming the primary computational tool for evaluating reaction rates and revealing the occurrence of nonintuitive atomistic processes at finite temperatures [11,12].

Accurate density-functional-based *ab initio* MD (AIMD) is limited, due to high computational cost, to the modeling of small systems (a few hundreds of atoms) during relatively short time frames (a few nanoseconds). Determining the rate of rare events via AIMD is a challenging task. Thus, one needs to resort to methods which can selectively accelerate a physical process of interest. The use of fictitious driving forces combined with a synthetic thermostat, which dissipates the energy increase due to external work, allows for accurately modeling a non equilibrium steady state via MD [13]. As long as the system's response to the applied constraint is linear, equilibrium (unconstrained) rates are reliably extrapolated from the results of non equilibrium MD [13,14]. However, restricting the acceleration method to linear-fitting ranges provides satisfactory gain in computational efficiency only for studying migration processes occurring with relatively high frequencies. Although, in general, deriving an analytical expression of the non equilibrium rate dependence on the intensity of external driving forces beyond the linear jump-rate vs force trend is a complex problem [13], in cases for which this dependence can be accurately modeled, equilibrium rates can be efficiently retrieved from nonlinear-range results.

With the color-diffusion (CD) algorithm [14,15], an extension of the tagged-particle method [16], an external constant force-field **F** is used to speed up migration of an atomic species while coupling all other particles to an isokinetic [17] thermostat. Recently, CD has been employed in non equilibrium AIMD (NE-AIMD) investigations of Li^+ migration in solid $LiBH_4$ [14] in which equilibrium diffusion coefficients are obtained by fitting linear-range results. However, tasks as, e.g., the estimation of vacancy diffusivities in crystalline solids, remain unfeasibly time consuming for NE-AIMD restricted to the CD linear-fitting regime.

In this paper, we show that, for cases in which atomic migration takes place over a single energy barrier (assumption typically valid for point-defect diffusion in crystal lattices [18–21] and adatom dynamics on surfaces [22,23]), equilibrium jump rates can be efficiently retrieved by fitting accelerated rates obtained within a sharply nonlinear jump rate vs force trend. To this aim, the CD algorithm is applied in NE-AIMD simulations of monovacancy jump in bcc Mo, here chosen as a model system. Numerical NE-AIMD experiments show that non equilibrium (accelerated) rates k_{NE} follow an Arrhenius-like behavior up to intensities F far beyond the linear range. We propose an analytical description for $k_{\mathrm{NE}}(F)$ which, at the limit of vanishing F, closely approaches nonaccelerated equilibrium rate (k_{E}) values. The extension of the CD method to the exponential regime translates, at

*Corresponding author: davsan@ifm.liu.se

simulation temperatures much lower than the melting point, in computational times several orders of magnitude smaller than those required in nonaccelerated dynamics.

II. COMPUTATIONAL DETAILS AND METHODS

AIMD runs are performed with VASP [24] using the projector augmented-wave method [25] and the Armiento-Mattsson functional (AM05) [26]. The equations of motion are integrated at 1-fs time intervals within the canonical ensemble NVT. At each time step, the total energy is evaluated to an accuracy of 10^{-5} eV/atom using a plane-wave energy cutoff of 400 eV while sampling the Brillouin zone Γ point. The electronic thermal excitations are modeled with electron-smearing energies corresponding to $k_B T$. In nonaccelerated simulations, prior to counting diffusion events, the lattice vibrations are allowed to stabilize for 4 ps by controlling the temperature via the Nosé-Hoover thermostat. The AM05 bcc Mo lattice parameter is only ∼0.5% smaller than the room-temperature experimental value (3.147 Å). This allows us to use experimental equilibrium volumes [27,28] for each simulation temperature. Simulation box sizes, 127 Mo atoms (n), and one vacancy ($4 \times 4 \times 4$ bcc unit cells), are sufficient to avoid point-defect self-interactions [29]. During both equilibrium and nonequilibrium simulations, vacancy jumps are identified from the variations in atomic positions (see Supplemental Material [30]).

The melting point T_{melt} of bcc Mo is ∼2900 K [28]. Simulation temperatures close to T_{melt} allow us to obtain well-converged AIMD vacancy jump rates k_{E}, defined as lattice-atom hops per time unit, which can be used to assess the accuracy of equilibrium rates $k_{\text{NE}\to\text{E}}$ extrapolated by NE-AIMD results. k_{E} is evaluated at temperatures of $T = 1600$, 1800, 2000, 2400, 2600, and 2800 K with simulation times of approximately 1.1, 0.7, 0.5, 0.1, 0.1, and 0.1 ns, respectively. Jump activation energies E_a and attempt frequencies A are obtained by fitting $\ln[k(T)]$ vs $1/T$ using the Arrhenius expression $k(T) = A\,\exp[-E_a/(k_B T)]$. Uncertainties on k, A, and E_a values are determined as described in Ref. [12].

Equilibrium rates calculated in this paper [$k_{\text{E}}(2800\,\text{K}) = 6.14(\times 1.2^{\pm 1}) \times 10^{11}\,\text{s}^{-1}$, $k_{\text{E}}(2600\,\text{K}) = 4.94(\times 1.2^{\pm 1}) \times 10^{11}\,\text{s}^{-1}$] compare well with those of previous AIMD estimations [$k_{\text{E}}(2800\,\text{K}) = 6.5(\times 2.0^{\pm 1}) \times 10^{11}\,\text{s}^{-1}$, $k_{\text{E}}(2600\,\text{K}) = 3.0(\times 2.0^{\pm 1}) \times 10^{11}\,\text{s}^{-1}$] [29]. The linear fit of $\ln[k_{\text{E}}(T)]$ vs $1/T$ yields $A = 44.9(\times 3.0^{\pm 1}) \times 10^{13}\,\text{s}^{-1}$ and $E_a = 1.58 \pm 0.25$ eV, in excellent agreement with the experimental value of $E_a = 1.62 \pm 0.27$ eV [31]. All Mo jumps recorded in AIMD runs occur among nearest-neighbor lattice sites; primary diffusion mechanism in bcc metals [32]. Thus, in this paper, we consider only ⟨111⟩ vacancy migration (see Supplemental Material [33]).

Color-diffusion applied to monovacancy migration in crystal lattices can be summarized as follows. Immersing a thermally equilibrated system in a constant force-field $\mathbf{F}$, the force acting on atom j is $c_j \cdot \mathbf{F}$ for which c_j (colors) are scalars. One lattice atom, referred to as *colored atom* ($c_1 = 1$), is pushed by a force $\mathbf{F}$ toward the neighboring vacancy while balancing forces $-\mathbf{F}/(n-1)$ act on all other atoms [$c_{2,\ldots,n} = -(n-1)^{-1}$]. The system temperature is controlled via rescaling all but the colored-atom velocities at each time step.

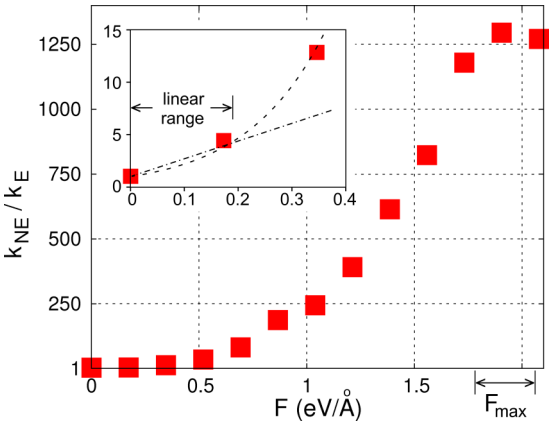

FIG. 1. Ratio of the NE-AIMD to AIMD jump rate $k_{\text{NE}}/k_{\text{E}}$ obtained as a function of F at 2000 K. The inset illustrates the linear-fitting range, previously used to extrapolate equilibrium rates [14].

For each force-field intensity F used at a temperature T, 19 initial NE-AIMD configurations are randomly selected out of 70 equilibrated states, in turn extracted every picosecond from AIMD runs. We use f values ($f = F/\sqrt{3}$ is the magnitude of ⟨100⟩ $\mathbf{F}$ components) in the ranges of 0.6–1.1 eV/Å with $T = 1000$, 1200, and 1400 K, 0.3–1.1 eV/Å with $T = 1600$ and 1800 K, and 0.1–1.6 eV/Å with $T = 2000$ K at f intervals of 0.1 eV/Å. Each NE-AIMD simulation is terminated when a neighboring Mo atom has migrated into the vacant site or when the simulation wall-time has been reached. k_{NE} is obtained by dividing the number (over all sample runs) of colored-atom jumps (multiplied by the number of nearest neighbors, eight, in bcc unit cells) by the total simulated time.

III. RESULTS

Figure 1 shows that the accelerated Mo vacancy jump rate $k_{\text{NE}}(F)$ calculated at 2000 K, normalized by the equilibrium $k_{\text{E}}(2000\,\text{K})$ value, follows an exponential-like dependence on F up to $F \cong 1.8$ eV/Å. NE-AIMD results at 1800 and 1600 K exhibit the same behavior. To clarify the effect of an applied force on the colored-atom jump rate, we use a simple TST-based one-dimensional model. Within the model, the zero-field effective potential-energy landscape E_{LS0} probed by the colored atom along a straight migration path $\mathbf{x}$ (see Supplemental Material [33]) is approximated by a sinusoidal function $E_{\text{LS0}}(x) = E_{a0}[-\cos(\pi x/x_{\text{TS0}}) + 1]/2$. Note that equilibrium (unperturbed) model quantities are indicated by subscripts ending with 0. $E_{\text{LS0}}(x)$ is characterized by two zero-energy minima: at the colored-atom initial ($x = x_{\text{eq}_0} = 0$) and final ($x =$ vacancy-site x_{vac}) equilibrium positions and one maximum of energy E_{a0} at the transition state $x = x_{\text{TS0}}$, midpoint of the diffusion path (Fig. 2).

The effect of an external force $\mathbf{F}$ (aligned with $\mathbf{x}$) on the perturbed potential-energy profile $E_{\text{LS}}(x)$ *seen* by the colored atom is interpreted as follows. After a short transient period, $E_{\text{LS}}(x)$ reaches a steady-state $E_{\text{LS}}(x,F) = E_{\text{LS0}}(x) - Fx$. For increasing intensities F, the colored-atom equilibrium

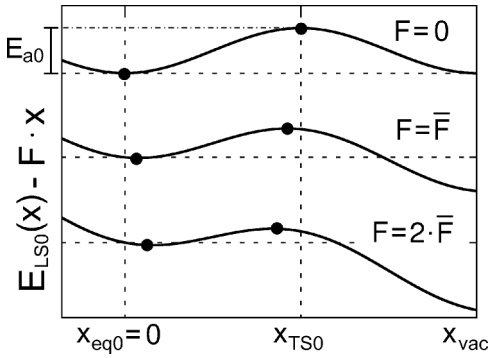

FIG. 2. Model used to clarify the colored-atom jump rate dependence on the intensity F of an applied force seen in Fig. 1. The unperturbed ($F = 0$) potential-energy profile $E_{\mathrm{LS}0}$ along the diffusion path x is approximated by a sinusoidal curve. With increasing force intensities F, the colored-atom equilibrium position x_{eq} and the transition-state coordinate x_{TS} move toward each other, whereas the effective jump activation energy E_a decreases monotonically. x_{eq_0}, $x_{\mathrm{TS}0}$, and E_{a0} are zero-field quantities. x_{vac} indicates the vacancy position.

position x_{eq} and the transition-state position x_{TS} shift continuously toward each other (Fig. 2). At the same time, the effective jump activation energy $E_a(F) = E_{\mathrm{LS}}[x_{\mathrm{TS}}(F), F] - E_{\mathrm{LS}}[x_{\mathrm{eq}}(F), F]$ becomes progressively smaller. The jump attempt frequency, approximated within the harmonic limit as $A(F) \propto \sqrt{[\partial^2 E_{\mathrm{LS}}(x,F)/\partial^2 x]_{x_{\mathrm{eq}}(F)}}$, decreases monotonically with increasing F due to the change in $x_{\mathrm{eq}}(F)$. When F reaches the value ($F_{\max}$) for which x_{eq} and x_{TS} meet at the sinusoidal-curve flex point, the harmonic approximation is no longer valid, and the model becomes dynamically unstable.

Starting from the unperturbed $E_{\mathrm{LS}0}(x)$ sinusoidal shape, we numerically evaluate the model accelerated-rate k dependence on F, $k(F) \propto A(F)\exp[-E_a(F)]$ for F varying up to $F_{\max}$ (Fig. 3). The model $k(F)$ vs F trends illustrated in Fig. 3 are consistent with those of NE-AIMD $k_{\mathrm{NE}}(F)$ values up to $F \cong 0.9\,F_{\max}$ (compare Fig. 3 with Fig. 1). Since the acceleration

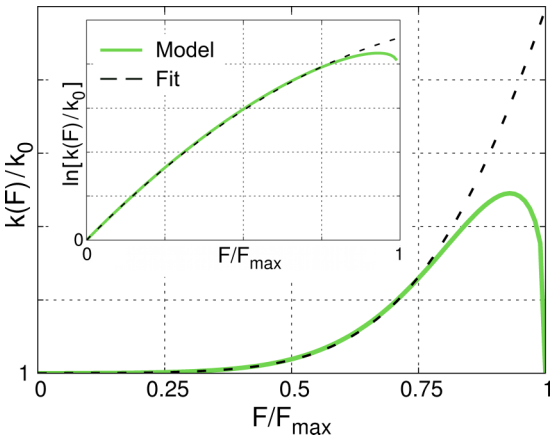

FIG. 3. Numerical evaluation of accelerated-rates $k(F)$ as a function of the intensity F of the force applied to the colored-atom based on the model illustrated in Fig. 2, and fit of $k(F)$ up to $F' \cong 0.75\,F_{\max}$ [Eqs. (1) and (2)].

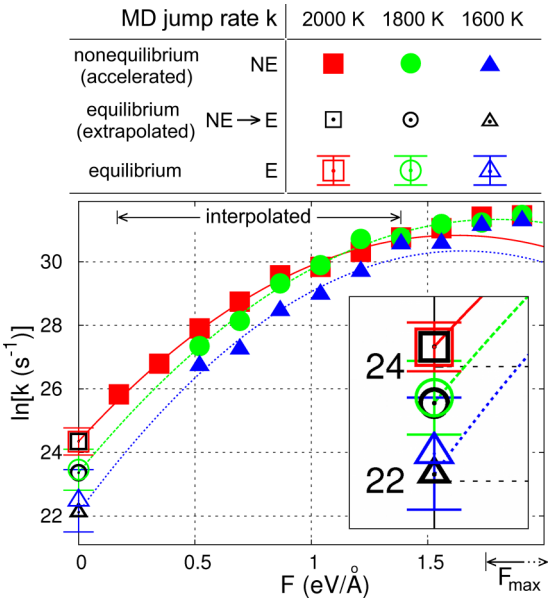

FIG. 4. Non equilibrium jump rates $\ln[k_{\mathrm{NE}}(F,T)]$ obtained as a function of F for $T = 1600$, 1800, and 2000 K. The inset illustrates the agreement between equilibrium rates $k_{\mathrm{NE}\to\mathrm{E}}$ extrapolated by non equilibrium k_{NE} results and equilibrium rates k_{E} obtained by nonaccelerated AIMD. $\ln(k_{\mathrm{E}})$ is shown with corresponding error bars. The force limit used for k_{NE}-result-fitting, as determined in our model calculations (Fig. 3), is $F' \cong 0.75\,F_{\max}$.

factor $k_{\mathrm{NE}}(F)/k_{\mathrm{E}}$ increases rapidly with F, Fig. 1, the aim is to describe $A(F)$ and $E_a(F)$ up to F close to $F_{\max}$.

Our analytical derivation of $A(F)$ and $E_a(F)$ based on the TST model can be found in the Supplemental Material in Ref. [30]. In synthesis, fitting the model k dependence on F with

$$k(F,T) = k_0(T)\exp\left[\frac{x_{\mathrm{TS}0}(T)}{k_B T}F - \alpha(T)F^2\right], \qquad (1)$$

where $\alpha(T)$ is a temperature-dependent parameter and k_0 is the equilibrium jump rate, reproduces the $k_{\mathrm{NE}}(F)$ trends up to $F' \cong 0.75 F_{\max}$ (Fig. 3). Taking the logarithm of both sides of Eq. (1) yields a polynomial $y_T(F)$,

$$\ln[k(F,T)] = \ln[k_0(T)] + \frac{x_{\mathrm{TS}0}(T)}{k_B T}F - \alpha(T)F^2. \qquad (2)$$

For fields of vanishing intensities, the slope of the parabola becomes $\lim_{F\to 0}\frac{\partial[y_T(F)]}{\partial F} = \frac{x_{\mathrm{TS}0}(T)}{k_B T}$. Setting $x_{\mathrm{TS}0}(T) = d_{\mathrm{NN}}(T)/2$ [for which $d_{\mathrm{NN}}(T)$, equilibrium nearest-neighbor distance at a temperature T, can be obtained, accounting for the thermal expansion by rescaling the 0 K d_{NN} value], the unknown parameters remaining in Eq. (2) are $\alpha(T)$ and the quantity of practical interest, the equilibrium jump rate $\ln[k_0(T)]$.

Let us return to *ab initio* simulations of vacancy migration in Mo. NE-AIMD jump rate $k_{\mathrm{NE}}(F,T)$ dependences on F plotted in Fig. 4 for $T = 1600$, 1800, and 2000 K, are consistent with those seen in our model calculations (Fig. 3). The results obtained at 1000, 1200, and 1400 K exhibit the same behavior. Although the actual 0-K energy profile along the reaction coordinate deviates from sinusoidal (see

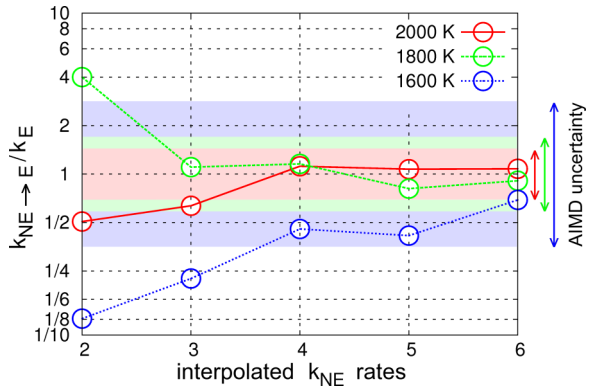

FIG. 5. Convergence of extrapolated equilibrium rates $k_{NE\to E}$, normalized by AIMD rate k_E values with the number of non equilibrium k_{NE} interpolation points. $k_{NE\to E}/k_E$ ratios are obtained for $f = 0.7$ and 0.8 eV/Å (two interpolated rates) and f ranging between 0.3 and 0.8 eV/Å (six interpolated rates). The vertical scale is logarithmic (base 10). Shaded red, green, and blue regions with limits marked by arrows (on the right) correspond to k_E error bars at 2000, 1800, and 1600 K, respectively.

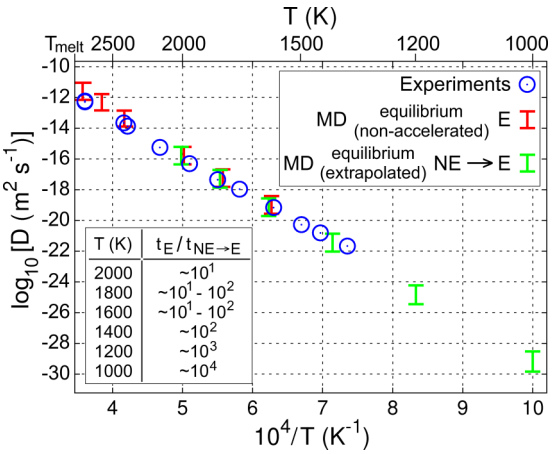

FIG. 6. Comparison between theoretical and experimental diffusion coefficients D [36]. The error bars on $D_E(T)[\propto k_E(T)c_V(T)]$ and $D_{NE\to E}(T)[\propto k_{NE\to E}(T)c_V(T)]$ values account only for the experimental uncertainty on equilibrium vacancy concentrations $c_V(T)$. The table in the inset lists the gain in computational efficiency $t_E/t_{NE\to E}$ achieved by our approach, where t_E and $t_{NE\to E}$ are approximate simulation times required to obtain well-converged equilibrium vacancy jump rates as a function of T in nonaccelerated AIMD and accelerated NE-AIMD simulations, respectively.

Supplemental Material [33]) [34], the expression in Eq. (2), based on a sine function model Hamiltonian, accurately reproduces the $k_{NE}(F)$ behavior up to F' at all temperatures.

At 2000 K, $x_{TS0} \cong 1.38$ Å. Using E_{a0} determined by AIMD, 1.58 ± 0.25 eV, in the expression $F_{max} = \frac{\pi E_{a0}}{2x_{TS0}}$ (see Supplemental Material [30]) yields $F_{max} = 1.80 \pm 0.25$ eV/Å; consistent with the force interval corresponding to zero slope in the $k_{NE}(F)$ curve of Fig. 1. If neither x_{TS0} nor E_{a0} vary significantly within the probed temperature range, F_{max} can be estimated by NE-AIMD at a given temperature and then assumed to remain constant. Thus, $F' \cong 1.4$ eV/Å ($\langle 100\rangle$ components $f' = 0.8$ eV/Å) is the maximum intensity used in the fit [Eq. (2)] of NE-AIMD results. The equilibrium rates ($k_{NE\to E}$) extrapolated from $k_{NE}(f)$ obtained within the range of $f = 0.1-0.8$ eV/Å are in excellent agreement with AIMD k_E values (inset in Fig. 4). This validates our approach and lends confidence that equilibrium rates can be reliably obtained by fitting non equilibrium results at all temperatures. It is worth stressing that the acceleration factor k_{NE}/k_E achieved in our approach increases rapidly for decreasing temperatures (Fig. 4); restricting CD, as done in previous investigations [14,35], to the narrow F interval yielding a *quasi*linear $k_{NE}(F)$ trend would provide considerably lower gain in computational efficiency (see inset in Fig. 1).

Extrapolated $k_{NE\to E}$ values progressively approach equilibrium AIMD rates k_E with an increasing number of $k_{NE}(f)$ interpolation points within the f range 0.8–0.3 eV/Å (Fig. 5). In fact, $k_{NE\to E}$ obtained by fitting just three $k_{NE}(f)$ points ($f = 0.6$, 0.7, and 0.8 eV/Å) falls within, or at least close to, AIMD uncertainty intervals. Thus, $f = 0.6$, 0.7, and 0.8 eV/Å is used to assess equilibrium rates at 1400, 1200, and 1000 K: $k_{NE\to E} = 8.2 \times 10^8$, 4.3×10^7, and 1.5×10^6 s^{-1}, respectively. At these temperatures, the estimation of vacancy jump rates via nonaccelerated dynamics would require simulation times of several microseconds. However, the use of the CD algorithm within the exponential regime reduces simulation times to a total of ~2 ns.

Finally, we compare the results of our approach with Mo vacancy diffusion coefficients $D(T)$ determined experimentally between 1350 and 2800 K [36]. Since $D(T) \propto k(T)c_V(T)$, the theoretical prediction of $D(T)$ requires the evaluation of vacancy equilibrium concentrations $c_V(T)$.

Glensk *et al.* [7], using *ab initio* calculations accounting for anharmonic effects, have shown that the temperature dependence of the Gibbs vacancy formation energy G^f in fcc Al and Cu is accurately described by $G^f(T) = H^f_{0K} - \frac{1}{2}T^2S'$, where $S' = \frac{\partial S^f}{\partial T}$ is a constant as the formation entropy $S^f(T) \cong TS'$ increases approximately linearly with T. The formation enthalpy H^f_{0K} of Mo vacancies estimated *ab initio*, 3.1 eV [29], is close to the experimental value of 3.24 ± 0.09 eV [31]. S' can be obtained from S^f measured at ~620 K [31] as $S' = [(2.6 \pm 0.4)\,k_B]/(620\,\text{K})$. Thus, using theoretical $k(T)$ values in the expression $D(T) = \frac{1}{6}\gamma d^2_{NN}(T)c_V(T)k(T)$, for which $c_V(T) = \exp[-G^f(T)/(k_BT)]$ and $\gamma = 0.72$ is the correlation factor for vacancy jump in bcc crystals [37], we determine $D(T)$ for T between 1000 and 2800 K. Calculated $D(T)$ values agree well with experimental results [36] at all temperatures (Fig. 6).

IV. CONCLUSIONS

To summarize, we show that the CD algorithm, employed in NE-AIMD simulations of Mo monovacancy diffusion accelerated by force fields reaching intensities far beyond the linear k vs F regime, allows reducing computational times by several orders of magnitude. The method is validated by comparing equilibrium jump rates extrapolated from the results of accelerated dynamics with nonaccelerated AIMD jump rates. The accuracy of extrapolated equilibrium rates can be improved systematically by increasing the number of NE-AIMD interpolation points, yet maintaining considerably

shorter computational times compared to those required in AIMD simulations. Our theoretical estimations of Mo vacancy diffusivities are in agreement with experimental results.

ACKNOWLEDGMENTS

The calculations and simulations were performed with resources provided by the Swedish National Infrastructure for Computing (SNIC) on the Gamma, Triolith, Matter, and Kappa Clusters located at the National Supercomputer Centre (NSC) in Linköping and on the Beskow cluster located at the Center for High Performance Computing (PDC) in Stockholm, Sweden. Dr. K. Finzel is acknowledged for useful discussions. W. Olovsson and P. Münger at NSC, and H. Leskelä and J. Vincent at PDC are acknowledged for assistance with technical aspects. We gratefully acknowledge financial support from the Knut and Alice Wallenberg Foundation (Isotopic Control for Ultimate Material Properties Project No. 2011.0094), the Swedish Research Council (VR) Grants No. 621-2011-4417, No. 2015-04391, No. 637-2013-7296, and No. 330-2014-6336, Linköping Linnaeus Initiative LiLi-NFM (Grant No. 2008-6572), and the Swedish Government Strategic Research Area Grant in Materials Science on Advanced Functional Materials (Grant No. MatLiU 2009-00971 through Sweden's innovation agency VINNOVA). I.A.A. is grateful for the Grant from the Ministry of Education and Science of the Russian Federation (Grant No. 14.Y26.31.0005) and Tomsk State University Academic D. I. Mendeleev Fund Program.

[1] C. Freysoldt, B. Grabowski, T. Hickel, J. Neugebauer, G. Kresse, A. Janotti, and C. G. Van de Walle, Rev. Mod. Phys. **86**, 253 (2014).
[2] F. Tuomisto and I. Makkonen, Rev. Mod. Phys. **85**, 1583 (2013).
[3] G. H. Vineyard, J. Phys. Chem. Solids **3**, 121 (1957).
[4] M. Mantina, Y. Wang, R. Arroyave, L. Q. Chen, Z. K. Liu, and C. Wolverton, Phys. Rev. Lett. **100**, 215901 (2008).
[5] N. Sandberg, B. Magyari-Köpe, and T. R. Mattsson, Phys. Rev. Lett. **89**, 065901 (2002).
[6] O. Hellman, P. Steneteg, I. A. Abrikosov, and S. I. Simak, Phys. Rev. B **87**, 104111 (2013).
[7] A. Glensk, B. Grabowski, T. Hickel, and J. Neugebauer, Phys. Rev. X **4**, 011018 (2014).
[8] H. M. Gilder and D. Lazarus, Phys. Rev. B **11**, 4916 (1975).
[9] O. Hellman, I. A. Abrikosov, and S. I. Simak, Phys. Rev. B **84**, 180301(R) (2011).
[10] A. B. Mei, O. Hellman, N. Wireklint, C. M. Schlepütz, D. G. Sangiovanni, B. Alling, A. Rockett, L. Hultman, I. Petrov, and J. E. Greene, Phys. Rev. B **91**, 054101 (2015).
[11] D. G. Sangiovanni, B. Alling, P. Steneteg, L. Hultman, and I. A. Abrikosov, Phys. Rev. B **91**, 054301 (2015).
[12] D. G. Sangiovanni, D. Edström, L. Hultman, I. Petrov, J. E. Greene, and V. Chirita, Surf. Sci. **624**, 25 (2014).
[13] D. J. Evans and G. Morriss, *Statistical Mechanics of Nonequilibrium Liquids*, 2nd ed. (Cambridge University Press, Cambridge, 2008).
[14] P. C. Aeberhard, S. R. Williams, D. J. Evans, K. Refson, and W. I. F. David, Phys. Rev. Lett. **108**, 095901 (2012).
[15] D. J. Evans, W. G. Hoover, B. H. Failor, B. Moran, and A. J. C. Ladd, Phys. Rev. A **28**, 1016 (1983).
[16] S. R. Williams and D. J. Evans, Phys. Rev. Lett. **96**, 015701 (2006).
[17] C. P. Dettmann and G. P. Morriss, Phys. Rev. E **54**, 2495 (1996).
[18] A. Janotti and C. G. Van de Walle, Phys. Rev. B **76**, 165202 (2007).
[19] M. Posselt, F. Gao, and H. Bracht, Phys. Rev. B **78**, 035208 (2008).
[20] Q. Shi, J. Voss, H. S. Jacobsen, K. Lefmann, M. Zamponi, and T. Vegge, J. Alloys Compd. **446**, 469 (2007).
[21] D. E. Jiang and E. A. Carter, Phys. Rev. B **70**, 064102 (2004).
[22] T. Olewicz, G. Antczak, L. Jurczyszyn, J. W. Lyding, and G. Ehrlich, Phys. Rev. B **89**, 235408 (2014).
[23] L. J. Xu, G. Henkelman, C. T. Campbell, and H. Jonsson, Surf. Sci. **600**, 1351 (2006).
[24] G. Kresse and J. Hafner, Phys. Rev. B **47**, 558 (1993).
[25] P. E. Blöchl, Phys. Rev. B **50**, 17953 (1994).
[26] R. Armiento and A. E. Mattsson, Phys. Rev. B **72**, 085108 (2005).
[27] K. Wang and R. R. Reeber, Mater. Sci. Eng., R **23**, 101 (1998).
[28] A. F. Guillermet, Int. J. Thermophys. **6**, 367 (1985).
[29] T. R. Mattsson, N. Sandberg, R. Armiento, and A. E. Mattsson, Phys. Rev. B **80**, 224104 (2009).
[30] See Supplemental Material at http://link.aps.org/supplemental/10.1103/PhysRevB.93.094305 for an analytical derivation of $A(F)$ and $E_a(F)$ based on the TST model.
[31] M. Suezawa and H. Kimura, Philos. Mag. **28**, 901 (1973).
[32] G. Neumann and V. Tölle, Philos. Mag. A **61**, 563 (1990).
[33] See Supplemental Material at http://link.aps.org/supplemental/10.1103/PhysRevB.93.094305 for nearest-neighbor and next nearest-neighbor vacancy jump activation energies calculated at 0 K with the nudged elastic band method.
[34] G. Mills, H. Jonsson, and G. K. Schenter, Surf. Sci. **324**, 305 (1995).
[35] A. D. Mulliner, P. C. Aeberhard, P. D. Battle, W. I. F. David, and K. Refson, Phys. Chem. Chem. Phys. **17**, 21470 (2015).
[36] K. Maier, H. Mehrer, and G. Rein, Z. MetaIlkd. **70**, 271 (1979).
[37] K. Compaan and Y. Haven, Trans. Faraday Soc. **52**, 786 (1956).